Ship twin-propeller jet model used to predict the initial velocity and velocity distribution within diffusing jet

Ship twin-propeller jet model used to predict the initial velocity and velocity distribution within diffusing jet

Jinxin Jiang[1 2]; Wei-Haur Lam*[1 2]; Yonggang Cui[1 2]; Tianming Zhang[1 2]; Chong Sun[1 2]; Jianhua Guo[1 2]; Yanbo Ma[1 2]; Shuguang Wang[1 2]; Gerard Hamill[3]

[1]State Key Laboratory of Hydraulic Engineering Simulation and Safety, Tianjin University, People's Republic of China
[2]First R&D Services, A-08-16 M Suites, 283 Jalan Ampang, 50450 Kuala Lumpur, Malaysia.
[3]School of Natural and Built Environment, Architecture, Civil & Structural Engineering and Planning, Queen's University Belfast, David Keir Building, Stranmillis Road, Belfast, BT9 5AG, United Kingdom.
Corresponding email: wlam@tju.edu.cn

Abstract: The current research proposed the theoretical model for ship twin-propeller jet based on the axial momentum theory and Gaussian normal distribution. The twin-propeller jet model is compared to the more matured single propeller jet model with good agreement. Computational Fluid Dynamics (CFD) method is used to acquire the velocity distribution within the twin-propeller jet for understanding of flow characteristics and validation purposes. Efflux velocity is the maximum velocity within the entire jet with strong influences by the geometrical profiles of the blades. Twin-propeller jet model showed four-peaked profile at the initial plane downstream to the propeller compared to the two-peaked profile from a single-propeller. The four-peaked profile merges to be two-peaked velocity profile and then one-peaked profile due to the fluid mixing. Entrainment occurs between the ambient still water outside and the rotating flow within jet due to the high velocity gradient. The research proposes a twin-propeller jet theory with a serial of equations enabling the predictions of velocity magnitude within the jet.

Keywords: Ship; Twin-propeller jet; Axial momentum theory; CFD

1. Introduction

Propeller is the most commonly used propulsion method for modern ships. A rotating propeller entrains the surrounding still water and subsequently ejects the water backward from a ship. Ship propels forward as reacting forces to allow the movement of a ship. The ejected water in the moving process is being called as ship propeller jet. This jet has high velocity characteristics with complicated rotating feature compared to a plain water jet. The impingement of this jet at the seabed close to harbour causes the seabed scouring leading to the sediment transport and damage of the harbour foundation. The investigations of the fluid flows within the ship's propeller wash which can lead to seabed scouring are of particular interest for the design of marine structures (Lam *et al.*, 2012).

The velocity of this jet decreases gradually with distances due to the mixing between the moving jet water and surrounding still water in an unrestricted area. If this jet is restricted, this high velocity jet will not decay naturally by entraining the surrounding water (Lam *et al.*, 2013). The high-speed jet causes seabed scouring when the natural dissipation of the energy is being restricted by the seabed. Natural mixing between the moving jet water and surrounding still water is being disturbed by balancing through the seabed sediment movement.

Size and rotational speed of a single propeller limit the propulsion system for a bigger ship. The twin-propeller system was proposed and being widely used to overcome the limitation of single propeller system. Two propellers are installed side by side at the stern of a ship instead of one propeller. Twin-propeller system provides more thrust compared to a single propeller. A ship can obtain more thrust from two installed propellers to allow the propulsion of a bigger ship.

The jets from twin-propeller system are not a simple combination of two single propeller jets. A single jet has three components of velocity, which are the axial, tangential and radial components of velocity (Lam *et al.*, 2013). Axial velocity leads to the axial motion of the jet as main contributor of the motion. Tangential velocity leads to the rotation of the jet and radial velocity leads to radial expansion of the jet. The interference of the two complicated propeller jets forms the twin-propeller jet, which has not much been reported by the previous researchers. The investigation is currently conducted to understand the nature of the twin-propeller jet and to propose a theoretical model to predict the velocity components of the jet.

Albertson *et al*. (1950) proposed a plain water jet theory to predict the velocity field based on axial momentum theory. Lee *et al*. (2003) summarised both jets and plumes and developed the theory about the interaction of multiple jets. Hamill (1987) measured the velocity distribution in the jet of a propeller model using Pitot tube and used the ship's propeller jet in the seabed scouring investigation instead of a plain water jet by the previous researchers. Lam *et al*. (2012) measured the axial, tangential and radial components of velocity at the efflux plane of a single propeller by using

Laser Doppler Anemometry (LDA) method. Hamill *et al.* (2015) investigated the efflux velocity from four different propellers operating at four rotational speeds and made comparison with the previous works. Hamill *et al.* (2016) proposed the semi-empirical equations to determine the location, magnitude and distribution of the axial velocity within a free expanding propeller jet. Mujal-Colilles *et al.* (2017) measured the velocity distribution within a twin-propeller jet using Acoustic Doppler Profiler (ADP) and suggested Blaauw *et al.*'s (1978) equation well agreed with the experimental results.

2. Methodology

Computational Fluid Dynamics (CFD) method is used to investigate the flow structure within twin-propeller jet. CFD is a numerical technique used to simulate the flow field based on Navier-Stokes equations through computer. CFD is inexpensive compared to the experimental method. Fundamental knowledge and governing equations of CFD can be learned in Versteegs and Malalasekera (2007). The well programmed CFD code ANSYS Fluent^{TM} (15.0) is used to solve the Navier-Stokes (NS) equations (ANSYS Fluent, 2013). The propeller geometry is created using Solidworks (Solidworks, 2016) and imported to ICEM^{TM} 15.0 modeller for mesh generation (ANSYS ICEM, 2013). Procedure of the geometry creation, mesh generation and solver solution are discussed in the following sections.

2.1 Geometry creation

A single propeller model with diameter of 76mm is selected in the current investigation. This propeller is termed as propeller-76 and was used in Lam (2008)'s PhD. Propeller-76 is arranged side by side virtually in CFD model to form the twin-propeller system. The characteristics of the propeller-76 can be found in Table 1 including the propeller diameter, hub diameter, blade number, rake angle, pitch ratio, blade area ratio, thrust coefficient. Diameter of twin-propeller (D_{tp}) is termed as the farthest distance between the tips of two propeller. The distance from hub to hub (L_h) is the distance between rotating central of two single-propeller. The distance from tip to tip (L_t) is the nearest distance between the tips of two propellers.

Table 1. Propeller characteristics of single-propeller and twin-propeller systems

Properties	**Single-propeller**	**Twin-propeller**
Propeller diameter, D_p (mm)	76	76
Hub diameter, D_h (mm)	14.92	14.92
Blade number, N	3	3
Rake angle, θ (°)	0°	0°
Pitch ratio (P')	1	1
Blade area ratio, β	0.473	0.473
Thrust coefficient, C_t	0.4	0.4
Diameter of twin-propeller, D_{tp} (mm)	-	228
Distance from hub to hub, L_h (mm)	-	152
Distance from inner tip to tip, L_t (mm)	-	76

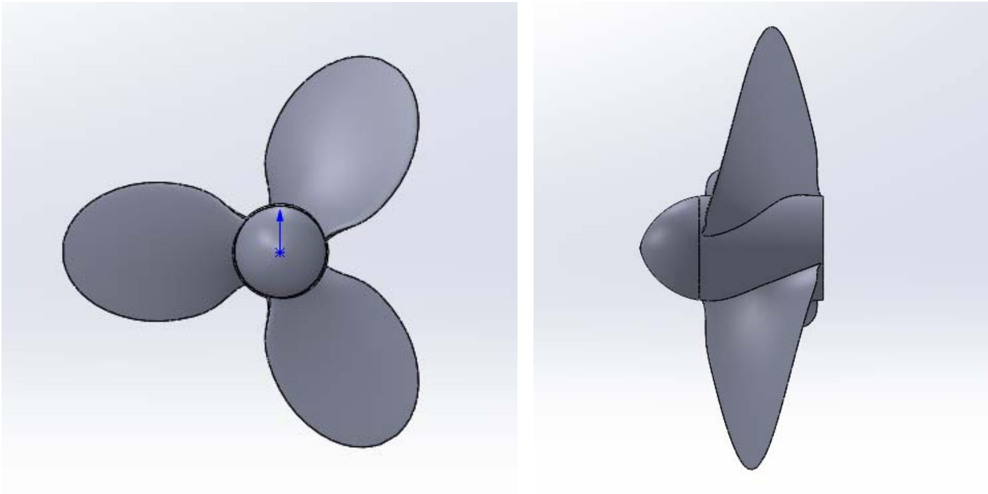

(a) (b)

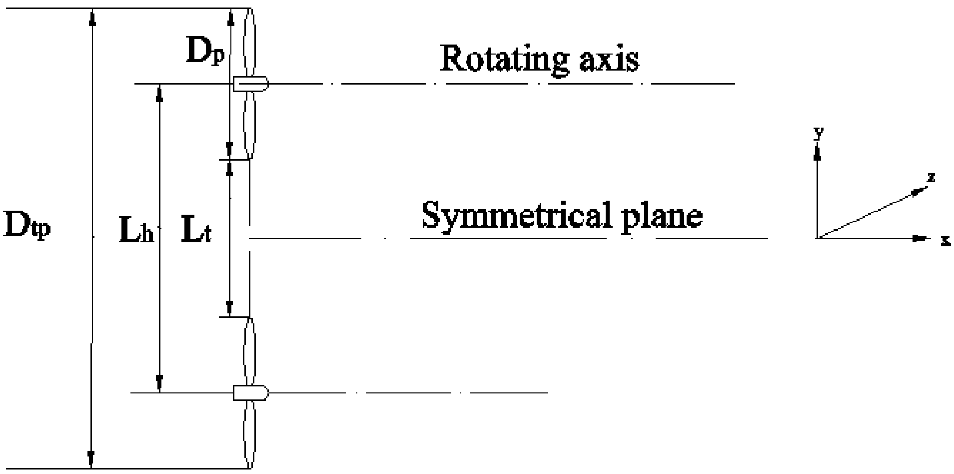

Fig. 1. Propeller geometry (a) aft view; (b) starboard view; (c) twin-propeller system

Solidwork is used to create the propeller geometry based on the propeller characteristics as presented in Table 1. Three-bladed propeller is shown in Fig. 1 as the aft view, starboard view and twin-propeller system. Two identical propellers are created side by side with one propeller diameter distance to form the twin-propeller system. The origin of coordinates is set at the midpoint of endpoints of two propellers' hubs as shown in Fig. 2 (a).

Domain is the boundary used for the automatic grid generation. Domain is divided to be rotor subdomain and water subdomain. Two cylinders termed as rotor subdomain surrounding the propellers are created to represent the rotating parts as rotor in the twin-propeller system. The two rotor subdomains are $1.2D_p$ in diameter and $1D_p$ in length. A bigger cuboidal subdomain is created to surround the cylinders with $52D_p$ in length, $14D_p$ in height and $16D_p$ in width. The cuboidal subdomain acts as the water domain as shown in Fig. 2.

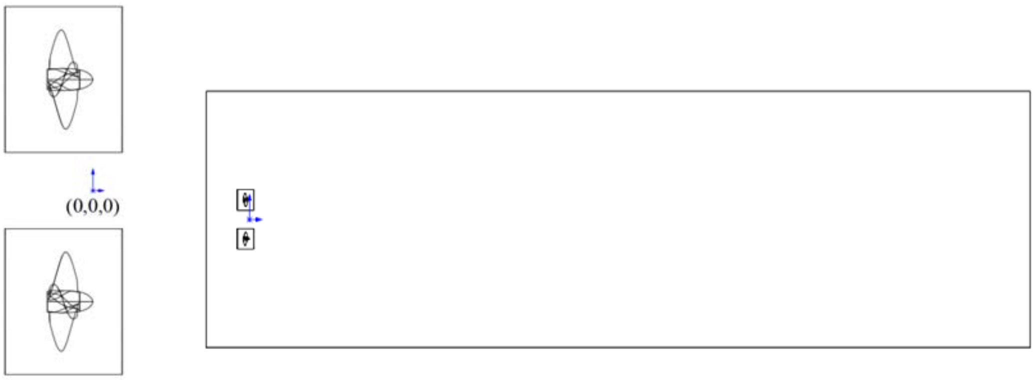

(a) (b)

Fig. 2. The rotating part and water domain surrounding the propeller (a) rotor subdomains (b) cuboidal subdomain

2.2 Grid generation

ICEM is used in the mesh generation in order to prepare the structured mesh for rotor subdomain and water subdomain. Structured grid is chosen to generate the grid for the twin-propeller model due to the consideration of accuracy. Mesh density is higher to capture the information close to the efflux plane regions, which is near to the propeller. Mesh for the twin-propeller system is shown in Fig. 3.

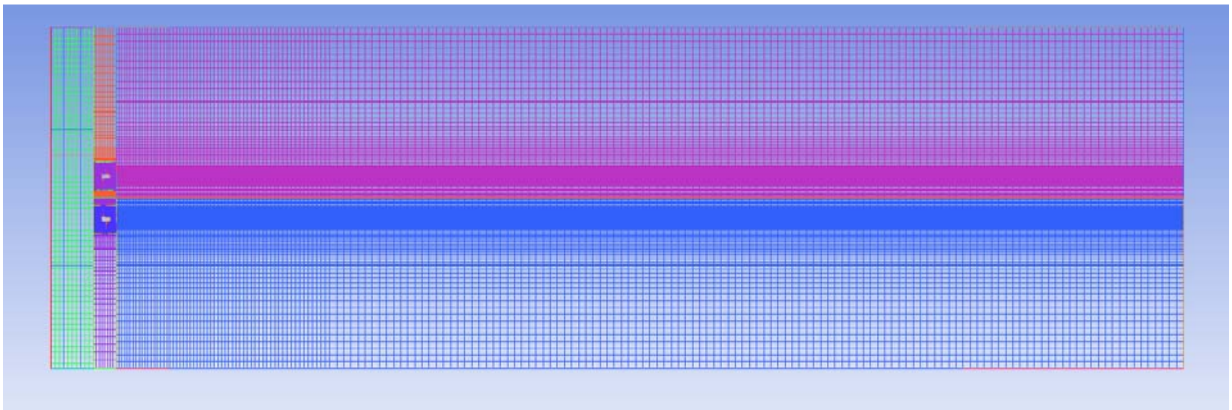

(a)

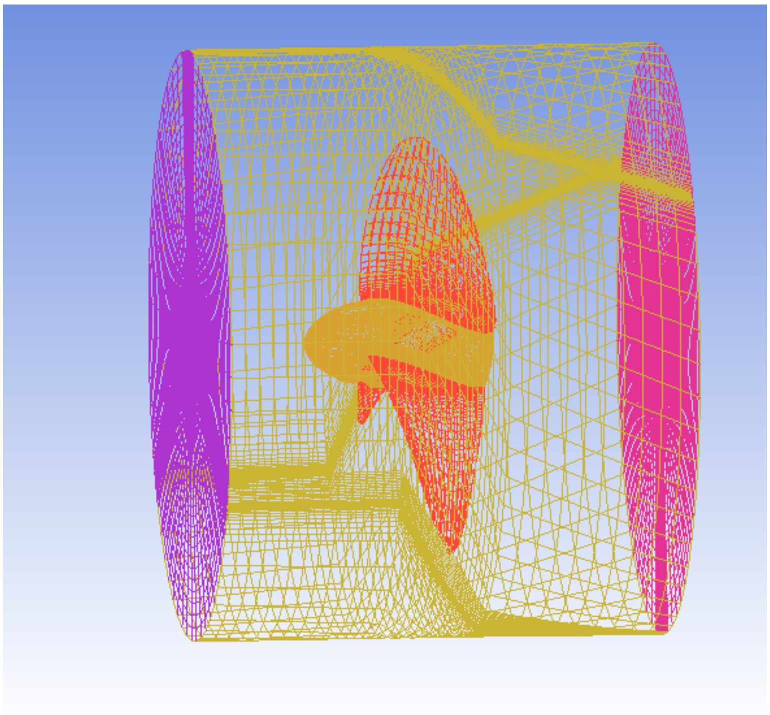

(b)

Fig.3. Water subdomain with embedded rotor subdomain (a) water subdomain; (b) rotor subdomain

2.3 Turbulence model and discretisation scheme

SST *k-ω* turbulence model is a time averaged turbulence model. SST k-ω turbulence model is more suitable for the calculation of propeller jet compared to most turbulence models such as standard k-ε model, standard k-ω model and Reynolds Stresses Model (RSM). SST k-ω turbulence model combines the positive features of both the standard k-ε model and standard k-ω model. The standard k-ω model can accurately predict the near-wall region and the standard k-ε model can accurately predict the far field. SST k-ω model combines these two models by a blending function F. SST k-ω model is equal to standard k-ω model at the near-wall region and is equal to standard k-ε model at the far field. SST k-ω model can both accurately predict the rotor subdomain and water subdomain in this case. More discussion on the turbulence models can be found in Versteegs and Malalasekera (2007).

Second order discretisation scheme is selected as in Lam (2008) instead of first order discretisation scheme. Discretisation scheme is used to calculate the velocity magnitudes through iteration process and the simulation is stopped at the designated under relaxation factor as converged results. Lam (2008) used the second order discretisation scheme in single-propeller jet calculation. The current study implements the second order scheme in twin-propeller jet as well. Second order discretisation scheme is selected to approximate the partial differential equations as algebraic equations over the discrete cells of the computational grid.

2.4 Mesh movement

Rotating reference frame is the method rotating the reference frame of the propeller relative to the inertial reference frame. Inertial reference frame is the global reference frame, which is always stationary. The water subdomain is located within the region of inertial reference frame. Rotating reference frame is used to rotate the propeller in rotor subdomains. This represents the physical motion of two rotating propellers. The water subdomain is connected to the rotor subdomain through interface, which is designed for two subdomains to exchange flow field information. Two propellers are rotating internally at opposite direction. Propellers are rotated using the rotating frame method at 1000 rpm as the setup in Lam (2008). Another two cases in which the propellers are rotating at 750 rpm and 1250 rpm are simulated as comparisons. The initial ambient velocity is zero in these three cases.

2.5 Domain sensitivity analysis

A domain sensitivity analysis is carried out to ensure the domain size giving insignificant influences to the model. Three domain sizes are tested. The first domain is $52D_p$ in length, $9D_p$ in height and $11D_p$ in width ($52\ D_p \times 9\ D_p \times 11D_p$). The second domain is $52D_p$ in length, $14D_p$ in height and $16D_p$ in width ($52\ D_p \times 14\ D_p \times 16\ D_p$). The third domain is $52D_p$ in length, $20D_p$ in height and $22D_p$ in width ($52\ D_p \times 20\ D_p \times 22D_p$). The maximum velocity values and average ambient velocity values at $x/D_p = 0, 4, 8, 14$ are compared in Table. 2. Domain independence reaches at the second domain. The second domain is used in the following investigation.

Table 2. The maximum velocity values and average ambient velocity values at $x/D_p = 0, 4, 8, 14$ in the three domains.

Type of velocity	**Size of domain in length, height and width (D_p)**	**Velocity at $0D_p$ (m/s)**	**Velocity at $4D_p$ (m/s)**	**Velocity at $8D_p$ (m/s)**	**Velocity at $14D_p$ (m/s)**
Maximum velocity	52×9×11	1.40	0.75	0.49	0.36
	52×14×16	1.40	0.75	0.49	0.36
	52×20×22	1.40	0.75	0.49	0.36
Average ambient velocity	52×9×11	0.05	0.05	0.08	0.1
	52×14×16	0.01	0.01	0.015	0.02
	52×20×22	0.01	0.01	0.015	0.02

2.6 Grid independence analysis

A grid independence analysis is carried out to ensure the grid refinement giving insignificant influences to the model. Three grid densities are tested including the 1010910-cell, 1542830-cell and 2474850-cell domains. The maximum velocity values at $x/D_p = 0, 4, 8, 14$ are compared in Table. 3. Grid independence reaches at the 1542830 cells. The 1542830-cell grid is used in the following investigation.

Table 3. The maximum velocity values at $x/D_p = 0, 4, 8, 14$ in the three cases with various grid densities.

Grid density	**Velocity at $0D_p$ (m/s)**	**Velocity at $4D_p$ (m/s)**	**Velocity at $8D_p$ (m/s)**	**Velocity at $14D_p$ (m/s)**
1010910-cell grid	1.39	0.74	0.51	0.39
1542830-cell grid	1.40	0.75	0.49	0.36
2474850-cell grid	1.40	0.75	0.49	0.36

3. Model validation

Lam (2008) investigated the axial, tangential and radial components of velocity within a single-propeller jet rotating at 1000 rpm by using a Laser Doppler Anemometry (LDA) system. Characteristics of the single-propeller jet are compared to the twin-propeller jet for validation purpose. A horizontal XY plane in Fig.4 is created in order to acquire the axial velocity, which is the main data for the comparison. Velocity in x-direction in the XY plane is the axial component of velocity. This investigation focuses on the time averaged axial velocity in twin-propeller jet. No data on the velocity distribution of the twin-propeller jet is found from the previous researchers. Twin-propeller jet is compared to the single-propeller jet using Lam's (2008) results.

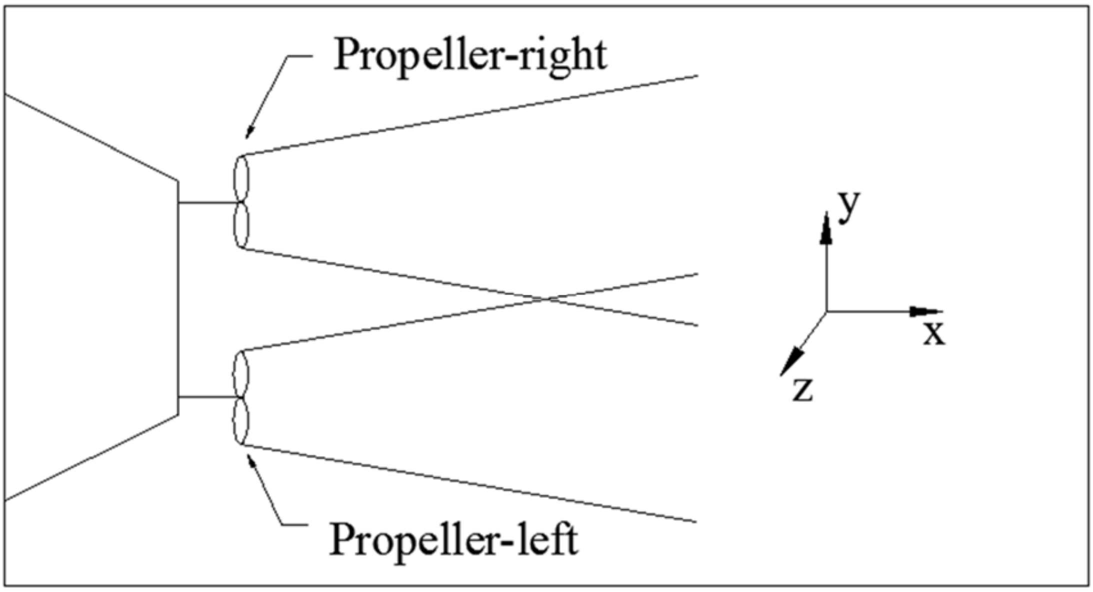

Fig.4. XY plane to acquire the axial velocity of twin-propeller.

Lam (2008) suggested that the maximum velocity occurs at the blade area with maximum thickness and zero axial velocity occurs at boundary of efflux plane $\frac{\mathrm{r}}{R_p} = 1.14$. No interference of two propellers is expected when the distance from hub to hub (L_h) is beyond the boundary of efflux velocity, which is two times of the boundary distance contributed by two propellers (2 x 1.14R_p= 2.28R_p). The current hub-to-hub (L_h) distance and inner tip-to-tip distance (L_t) are $4R_p$ and $2R_p$ respectively, which is far enough to prevent the interference. The velocity of the inner tip-to-tip at the efflux plane is close to zero and little disturbance occurs between the two single-propellers in twin-propeller at the efflux plane. The twin-propeller at efflux plane can be regarded as two non-interfering single propellers. Twin-propeller results can be validated by using the LDA results of single propeller at efflux plane.

3.1 Single propeller jet theory

Fuehrer and Romisch (1977) defined the efflux velocity (V_0) as the maximum velocity at the face of the propeller. Theoretical equation derived from axial momentum theory Eq. (1) is a widely accepted equation used to predict efflux velocity, as shown in Table 4. Hamill (1987) conducted experiments and proposed a correction factor 1.33 instead of 1.59 to propose Eq. (2). Stewart (1992) further refined Eq. (1) by including the consideration of the propeller diameter, pitch ratio and blade area ratio to calculate the efflux coefficient as Eq. (3).

Table 4. Prediction of efflux velocity

Source	**Equations**	
Axial momentum theory	$V_0 = 1.59 n D_p \sqrt{C_t}$	Eq. (1)
Hamill (1987)	$V_0 = 1.33 n D_p \sqrt{C_t}$	Eq. (2)
Stewart (1992)	$V_0 = \varsigma n D_p \sqrt{C_t}$ $\varsigma = D_p^{-0.0686} P'^{\,1.519} \beta^{-0.323}$	Eq. (3)

Hamill (1987) suggested that the velocity of the lateral distribution from efflux plane to $0.5D_p$ downstream of the propeller can be predicted using Eq. (4).

$$\frac{V_{x,r}}{V_{max}} = e^{[-(1/2)((r-R_{mo})/(R_{mo}/2))^2]} \qquad \text{Eq. (4)}$$

where $V_{x,r}$ is the mean velocity at any position in the jet defined by the axial direction x from the initial efflux plane and the radial distance r from the rotation axis.

V_{max} is the maximum velocity of the cross section. R_{mo} is the radius distance from the rotating axis to the point of maximum axial velocity at the efflux plane, which can be calculated based on the equations in Table 5.

Table 5. Prediction of the position of efflux velocity

Source	**Equation**	
Berger *et al*. (1981)	$R_{mo} = 0.67(R_p - R_h)$	Eq. (5)
Prosser (1986)	$R_{mo} = 0.6(R_p - R_h)$	Eq. (6)
Hamill (1987)	$R_{mo} = 0.7(R_p - R_h)$	Eq. (7)

Where R_p is the radius of propeller and R_h is the radius of the propeller hub.

Berger *et al*. (1981) proposed the position of the efflux velocity occurs at a distance 0.67 of blade area from the rotation axis to propose Eq. (5) as shown in Table 5. Propeller blade is being carefully designed with the hydrofoil geometry and the hub is only used to connecting the blade. The equation only considers the blade region without the hub region. Stewart (1992) agreed the equation proposed by Berger *et al*. (1981). Prosser (1986) and Hamill (1987) corrected the equations with a close coefficient 0.6 and 0.7 respectively, as Eq. (6) and (7) in Table 5.

3.2 Validation at the efflux plane

Fig. 5 shows comparison of the twin-propeller system with the previous single propeller works from Lam (2008) and Hamill (1987). The efflux plane is set at the aforementioned origin of coordinates. In this study, the central axis is set at y/R_p=0 in twin-propeller system. The rotational axes are set at $y/R_p = -2$ for left prop-76 and $y/R_p = 2$ for right prop-76. Efflux velocity (V_0) and its position (R_{mo}) are acquired from the current numerical results. These values are included as an input for Eq. (4) to obtain the entire axial velocity distribution based on Hamill (1987)'s equation. Lam (2008)'s experimental results are acquired directly from the previous works for comparison. Current CFD results are acquired using the post-processing function in Fluent.

The axial velocity distribution of twin-propeller at the efflux plane is the same as two single propellers as shown in Fig. 5. The current CFD results (1000 rpm) shows good agreement with the Lam (2008)'s experimental measurements and Hamill (1987)'s works. Five results show similar trend with four peaks and the axial velocity from -$1R_p$ to $1R_p$ is close to zero with no interference between two propellers at the efflux plane. The comparison of efflux velocity and its position between the current CFD results and the previous works are presented in Tables 6 and 7. The variations of the efflux velocity are 9.3%, 23.7%, 12.1% and 2.5% respectively when comparing the current results with the axial momentum theory, Hamill (1987), Stewart (1992) and Lam (2008), as shown in Table 6. The position of efflux velocity has variation of 1.8%, 12.7%, 1.8% and 7% compared to Berger *et al.* (1981), Prosser (1986), Hamill (1987) and Lam (2008), as shown in Table 7.

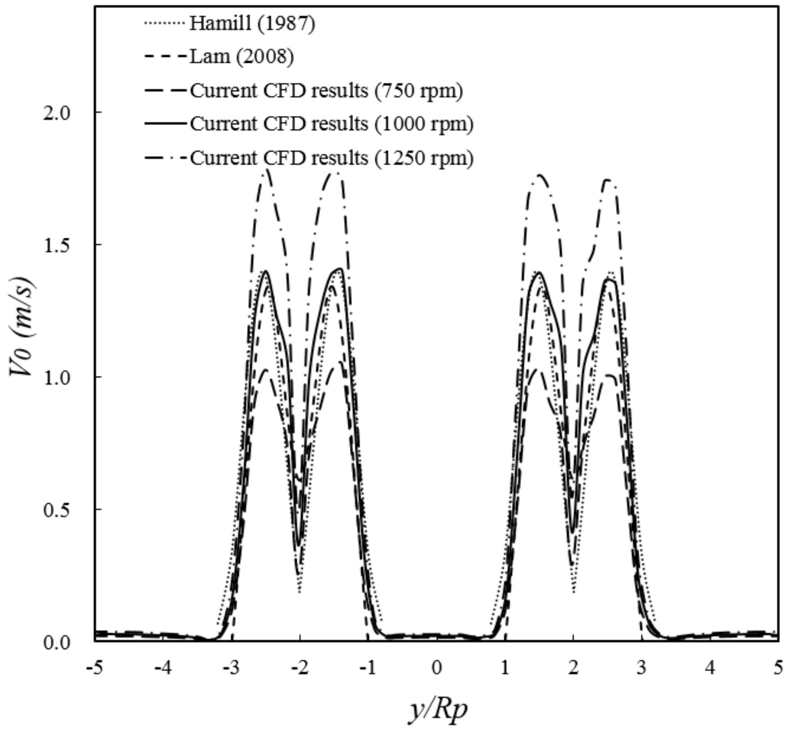

Fig. 5. Comparison of the velocity distribution at efflux plane for the current CFD results, Lam (2008) and Hamill (1987)

Table 6. Comparison of efflux velocity

Sources	**Efflux velocity (m/s)**	**Variation (%)**
Axial momentum theory	1.27	9.3
Hamill (1987)	1.067	23.7
Stewart (1992)	1.23	12.1
Lam *et al.* (2008)	1.365	2.5
Current CFD results (1000 rpm)	1.40	-
Current CFD results (750 rpm)	1.05	25
Current CFD results (1250 rpm)	1.78	27

Table 7. Comparison of the position of efflux velocity

Sources	**Radius position of peaked value (r/R_p)**	**Variation (%)**
Berger *et al*. (1981)	0.56	1.8
Prosser (1986)	0.48	12.7
Hamill (1987)	0.56	1.8
Lam *et al.* (2008)	0.59	7
Current CFD results (1000 rpm)	0.55	-
Current CFD results (750 rpm)	0.55	0
Current CFD results (1250 rpm)	0.55	0

Table 6 shows the efflux velocity of theoretical results (axial momentum theory) matches well with the experimental results in Lam *et al.* (2008) and the current CFD results. Variation between the theoretical results and experimental results is 2.5%, while the variation between the theoretical theory and CFD results is 9.2%. Two variations are less than 10% and it is in an acceptable range as common engineering practise. Eq. (1) from axial momentum theory is suitable for efflux velocity prediction in twin-propeller as well. CFD prediction shows agreement with the equation proposed by Berger et al. (1981), Prosser (1986), Hamill (1987) and Lam (2008) with variations of 1.8%, 12.7%, 1.8% and 7% for the position prediction as shown in Table 7. The current CFD results fit well with Berger *et al.* (1981) Prosser (1986) , Hamill (1987), Stewart (1992) and Lam (2008).

The axial velocity distribution patterns of the three rotating speed cases at 750 rpm, 1000 rpm and 1250 rpm are similar at the efflux plane as shown in Fig. 5. The efflux velocities are 1.05m/s, 1.4m/s and 1.78m/s when the rotating speeds are 750 rpm, 1000 rpm and 1250 rpm, as shown in Table 6. The efflux velocity of twin-propeller is direct proportional to the rotating speed. These three cases have the same peaked value position of efflux plane at $0.55R_p$ as shown in Table 7. The radius position of peak value is independent to the rotating speed at the efflux plane.

4. Results and discussions

The flow field behind a manoeuvring ship is the combination from a rotating propeller jet and turbulent wake from the hull, which is complicated. The turbulent wake from the hull is small that it can be ignored when the ship is stationary at the harbour, (Prosser, 1986). The flow field behind the ship is more complex than single propeller ship when it is a twin-propeller ship. The turbulent wake from the hull could also be ignored when the ship berths at the harbours. The flow field behind the manoeuvring twin-propeller ship can be simplified as the jet of twin-propeller.

For twin-propeller, the flow field is different from the single propeller. The time averaged axial velocity in the jet of single propeller is axisymmetric under all rotational speeds about the rotational axis. However, this axisymmetrical condition does not exist for twin-propeller due to the influence of the propellers side by side.

The twin-propeller jet is symmetric about the vertical and horizontal symmetrical planes. The jet at the horizontal symmetrical plane is the most representative plane in the flow field. Data are acquired from this plane for the following investigations. The proposed flow structure of the twin-propeller jet is presented in Fig. 6 based on the numerical results.

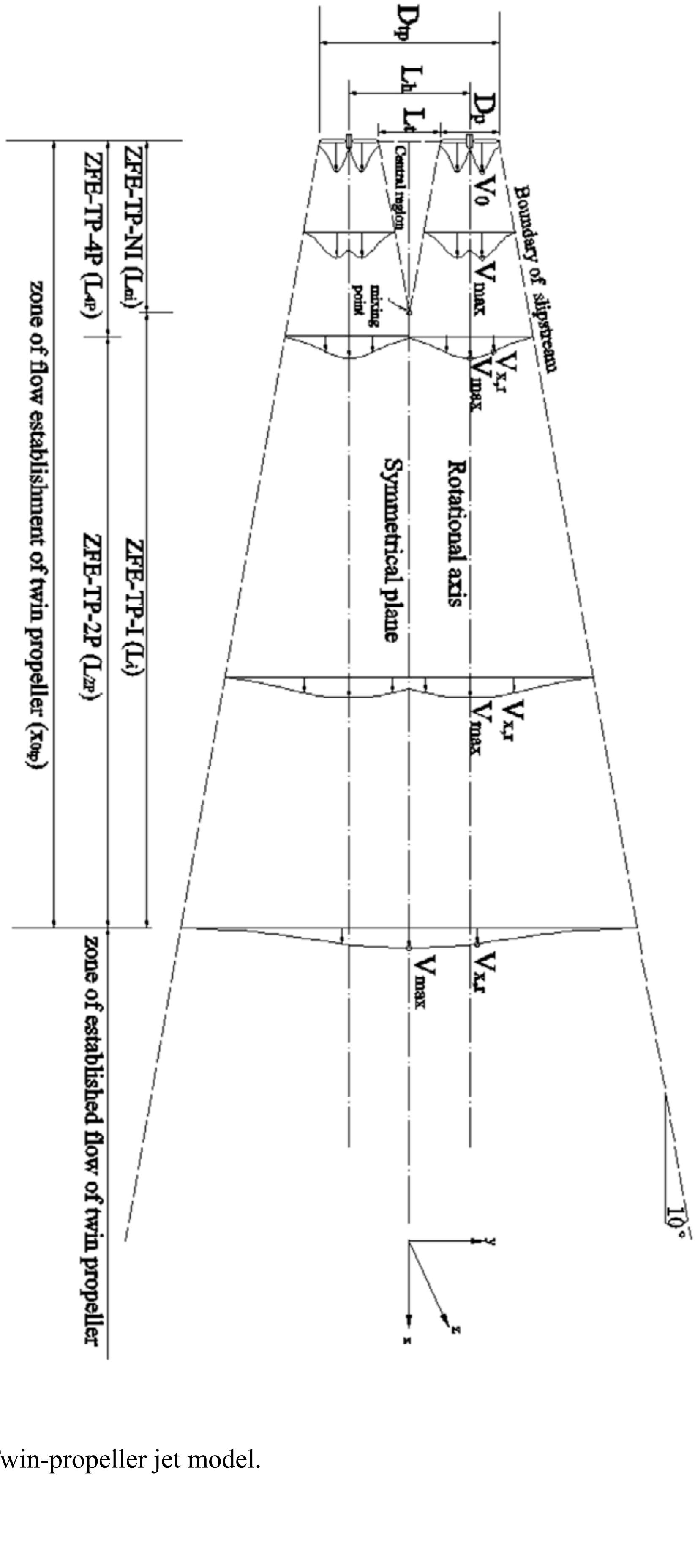

Fig. 6. Twin-propeller jet model.

4.1 Length of zone of flow establishment of twin-propeller.

For single propeller, Hamill (1987) stated that the zone of flow establishment of single propeller is the zone at which there are two peak values at the lateral distribution of axial velocity and a lower velocity core at the rotation axis. The two peaks merge into one peak at the rotation axis at the end of the zone of flow establishment of single propeller ($\mathrm{x} = x_0$). The remaining region downstream is the zone of established flow of single propeller. Blaauw & van de Kaa (1978), Fuehrer *et al.* (1981), Verhey (1983), Hamill (1987), Stewart（1992）proposed the length of the zone of flow establishment is $2.18D_p$、$2.60D_p$、$2.77D_p$、$2.00D_p$ and $3.25D_p$. Hamill (2016) validated the result of Stewart (1992) by experiments.

The number of peak values of twin-propeller decreases with the jet development downstream, which is analogous to the flow field from a single propeller. All the peak values merge into one in the zone of established flow. Albertson *et al.* (1950) proposed that the diffusion process continues thereafter without essential change in character in the zone of established flow. The zone with only one peak value in the flow field of twin-propeller is defined as the zone of established flow, and the upstream zone is the zone of flow establishment.

There are four peak values at the efflux plane. Then four peak values merge into two peak values at $\mathrm{x} = x_0$ from the efflux plane. It is zone of flow establishment of twin-propeller with 4 peak values (ZFE-TP-4P), whose length is L_{4p}. The two peak values merge into one peak value at the symmetrical plane (x = x_{0tp}). It is the end of the zone of flow establishment of twin-propeller. The zone from x_0 to x_{0tp} is zone of flow establishment of twin-propeller with 2 peak values (ZFE-TP-2P), whose length is L_{2p}. The zone of flow establishment of twin-propeller is made up of ZFE-TP-4P and ZFE-TP-2P. The rest zone downstream of $x = x_{0tp}$ is the zone of established flow.

Three numerical cases rotating at 750rpm, 1000rpm and 1250rpm show that the four peak values merge into two at $x_0 = 3.5D_p$, which is close to the Stewart's（1992） result of $3.25D_p$. In general, the length of ZFE-TP-4P has little difference with the length of zone of flow establishment in single propeller jet. The interference of two propeller jets is negligible within this zone. The length of ZFE-TP-4P is independent to the rotational speed of propeller. Therefore, the previous proposals of single propeller jet are suitable in predicting the length of ZFE-TP-4P in the twin-propeller jet.

The two propellers do not influence each other at the efflux plane. This condition continues up to a mixing point at the boundaries of two propeller jet. The zone from the efflux plane to the mixing point is called non-interference zone (ZFE-TP-NI, L_{ni}). The zone from mixing point to the end of the zone of flow establishment is called interference zone (ZFE-TP-NI, L_i). Johnston *et al*. (2013) indicated that the diffusion angle of single propeller jet is 10°. The length of none interference zone (L_{ni}) can be proposed based on this conclusion giving Eq. (8).

$$L_{ni} = \frac{L_t}{2*tan10^{\circ}} = 2.84L_t \quad (8)$$

The two propeller jets influence each other within the interference zone and finally merge into one peak value at the symmetrical plane in the end of the zone of flow establishment. Numerical results under all rotational speeds of 750rpm, 1000rpm and 1250rpm showed that the zone of flow establishment ends at $x_{0tp} = 14D_p$. The length of zone of flow establishment of twin-propeller is independent to the rotational speeds of propeller. In addition, the length of zone of flow establishment (x_{0tp}) is influenced by the distence from hub to hub (L_h). Two peaks at ZFE-TP-2P would never merge into one peak value if L_h is long enough. The value of x_{0tp} would be infinite if L_h is long enough. CFD results showed the length of zone of flow establishment (x_{0tp}) is 14D_p when the distence from hub to hub (L_h) is 2D_p.

4.2 Maximum velocity decay within the zone of flow establishment

The peak values do not merge into one within the zone of flow establishment of twin-propeller jet. The maximum axial velocity at the peak values of two propellers has little influence to the each other. Therefore, the magnitude of the maximum axial velocity decay within the zone of flow establishment of twin-propeller jet should be the same as single propeller. The equations of the maximum axial velocity decay of single propeller jet are suitable for twin-propeller jet within the zone of flow establishment.

The previous researches proposed the equations used to predict the maximum axial velocity decay within the zone of flow establishment and the zone of established flow from a single propeller, as shown in Tables 8 and 9. Verhey (1983) found that the maximum axial velocity decays in an exponential form of Eq. (12) within the zone of established flow. Stewart (1992) found that the velocity decays in a linear relationship with $\frac{x}{D_p}$ and proposed Eqs. (9) and (14) to describe the maximum axial velocity decay within the zone of flow establishment and the zone of established flow of single propeller. Lam *et al*. (2011) proposed Eq. (10) to predict the maximum axial velocity decay within the zone of flow establishment based on experiment. Hamill (2016) proposed Eqs. (11) and (13) to predict the maximum axial velocity decay within the zone of flow establishment and the zone of established flow of single propeller based on the experimental data.

Table 8. Predictions of the maximum axial velocity decay within the zone of flow establishment of single propeller.

Sources	**Equations**
Stewart (1992)	$0 \leq x/D_p < 3.25$ $\frac{V_{max}}{V_0} = 1.0172 - 0.1835(\frac{x}{D_p})$ Eq. (9)
Lam *et al*. (2011)	$0 \leq x/D_p < 3.68$ $\frac{V_{max}}{V_0} = 1 - 0.1592(\frac{x}{D_p})$ Eq. (10)
Hamill (2016)	$0 \leq x/D_p < 0.35$ $\frac{V_{max}}{V_0} = 1$

	$0.35 \leq x/D_p < 3.25$ $\frac{V_{max}}{V_0} = 1.51 - 0.175\left(\frac{x}{D_p}\right) - 0.46P^{\prime}$ Eq. (11)

Table 9. Predictions of the maximum axial velocity decay within the zone of established flow of single propeller.

Sources	**Equations**
Verhey (1983)	$1.5 \leq x/D_p$ $\frac{V_{max}}{V_0} = 1.275(x/D_p)^{-0.7}$ Eq. (12)
Hamill (2016)	$3.25 \leq x/D_p$ $\frac{V_{max}}{V_0} = 0.964 - 0.039\left(\frac{x}{D_p}\right) - 0.344P^{\prime}$ Eq. (13)
Stewart (1992)	$3.25 \leq x/D_p$ $\frac{V_{max}}{V_0} = 0.543 - 0.0281\left(\frac{x}{D_p}\right)$ Eq. (14)

The theoretical predictions, the experimental results of single propeller from Lam (2008) and the current numerical results are compared to predict the maximum axial velocity decay within the zone of flow establishment of twin-propeller jet, as shown in Fig.7. Stewart (1992) reported the decay of the maximum axial velocity of single propeller jet is independent of the speeds of rotation and current CFD results agreed with Stewart (1992)'s proposal. The current three numerical cases rotating at 750 rpm, 1000 rpm and 1250 rpm show similar maximum axial velocity decay with less than 5% variation, as shown in Fig. 7. It can be concluded that the maximum velocity decay of twin-propeller jet is independent of the speeds of rotation. It is noted that the value of experimental results are less than the numerical results before $x_0 = 3.5D_p$. Eq. (11) from Hamill (2016) is recommended to predict the maximum axial velocity decay within ZFE-TP-4P by comparing the numerical value in Fig 7.

The variation between the experimental results and the numerical result is in an acceptable range within the zone downstream of $x_0 = 3.5D_p$. Eq. (12) from Verhey (1983) is recommended to predict the maximum axial velocity decay within ZFE-TP-2P by comparing the numerical value in Fig 7. In general, the numerical results are larger than the experimental results and theoretical results. This maybe due to the interaction between two propellers during the jet development downstream.

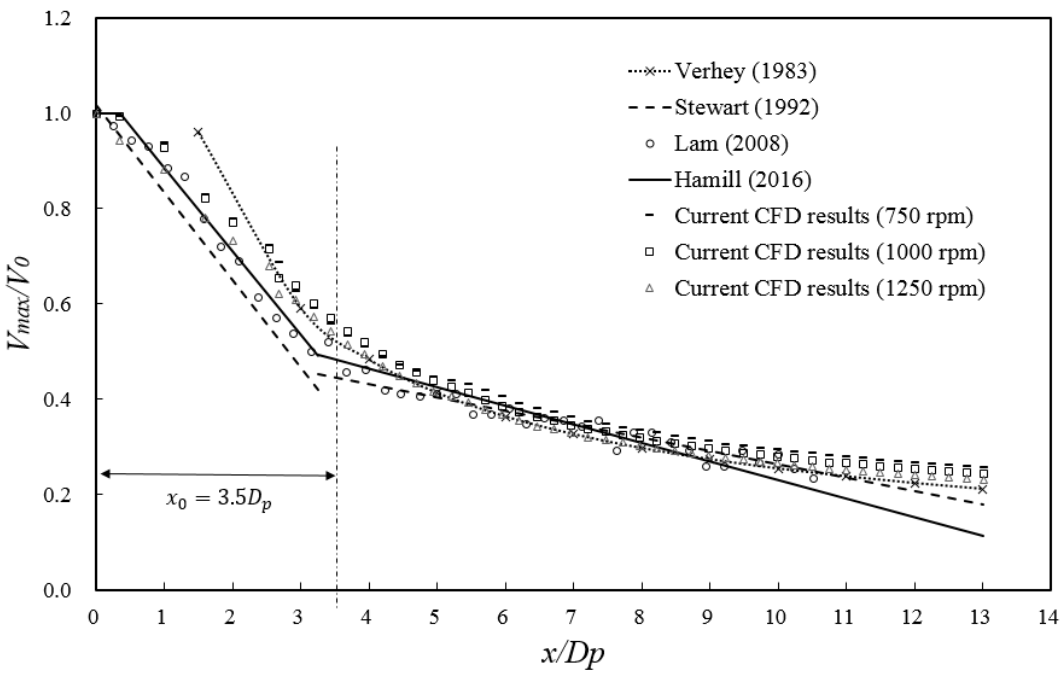

Fig. 7 Comparison of the maximum axial velocity decay within the zone of flow establishment

4.3 Maximum velocity decay within the zone of established flow

Albertson *et al*. (1950) proposed that the momentum flux is a constant for all normal sections of propeller jet. Based on this theory, the momentum flux of the one peak value within the zone of established flow is equal to the sum of the momentum flux of peak value of two single propellers giving Eq. (15).

$$\rho \Delta S V_{tpmax}^2 = 2\rho \Delta S V_{spmax}^2 \quad \text{Eq. (15)}$$

where V_{tpmax} is the magnitude of the maximum axial velocity within the zone of established flow of twin-propeller jet. V_{spmax} is the magnitude of the maximum axial velocity within the zone of established flow of single propeller jet at the same cross section. ρ is the density of fluid. ΔS is the area of a area element at the positon of the maximum velocity.

Substituting Eq. (12) into Eq. (15), the magnitude of the maximum axial velocity decay within the zone of established flow of twin-propeller jet can be described by Eq. (16), which is also called Jiang and Lam equation.

$$\frac{V_{max}}{V_0} = 1.8\left(\frac{x}{D_p}\right)^{-0.7} \quad \text{Eq. (16)}$$

Fig. 8 compares the theoretical results with the numerical results about the maximum axial velocity decay within the zone of established flow of twin-propeller jet. Three numerical cases rotating at 750 rpm, 1000 rpm and 1250 rpm show similar maximum axial velocity decay with the maximum variation less than 5%. It can be concluded that the maximum velocity decay of twin-propeller jet is independent of the speeds of rotation within the zone of established flow. It is noted that the values of theoretical predicted results are less than the numerical results before $x = 18D_p$, with the maximum variation of 9.6% at $x = 14D_p$. This may be due to the incomplete merging of two propeller jets within the zone, where the peak value decreases continously. The theoretical results within the zone downstream of $x = 18D_p$ matches well with the numerical results with the maximum variation of 7%.

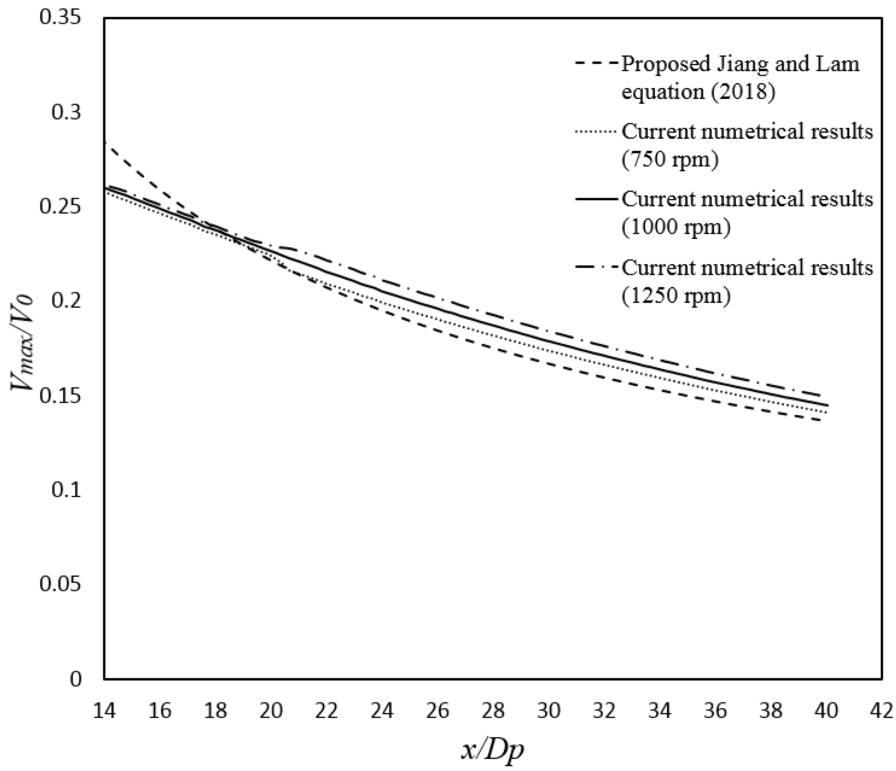

Fig. 8. Prediction of the maximum axial velocity decay within the zone of established flow

4.4 Velocity distribution within zone of flow establishment

Albertson *et al*. (1950) proposed that the velocity distribution at any sections of single propeller jet follows the general trend of the Gaussian normal probability function, which is also suitable in the velocity distribution of twin-propeller jet.

4.4.1 Four-peaked region

Hamill (1987) proposed Eq. (17) based on the Albertson *et al.* (1950)'s works to predict the axial velocity distribution within the zone of flow establishment of single propeller.

$$\frac{V_{x,r}}{V_{max}} = e^{\left[-\frac{1}{2}\frac{(r-R_{m0})^2}{\sigma^2}\right]} \qquad \text{Eq. (17)}$$

σ is standard deviation, and the value of it is decided by the position of the section. The value of σ is determined by Eqs. (18) and (19).

$$\sigma = \frac{1}{2}R_{m0}, \text{ for } \frac{x}{D_p} < 0.5 \qquad \text{Eq. (18)}$$

$$\sigma = \frac{1}{2}R_{m0} + 0.075\left(x - \frac{D_p}{2}\right), \text{ for } \frac{x}{D_p} > 0.5 \qquad \text{Eq. (19)}$$

Fig. 9 illustrates the properties of the lateral velocity distribution at 1.6 D_p downstream within ZFE-TP-4P. The maximum mean velocity of the jet at each sections is firstly obtained from the CFD results (1000 rpm). This value is included as an input for Eq. (17) to predict the axial velocity distribution for the twin-propeller Lam (2008)'s single propeller experimental results are mirrored to produce the velocity distribution of twin-propeller.

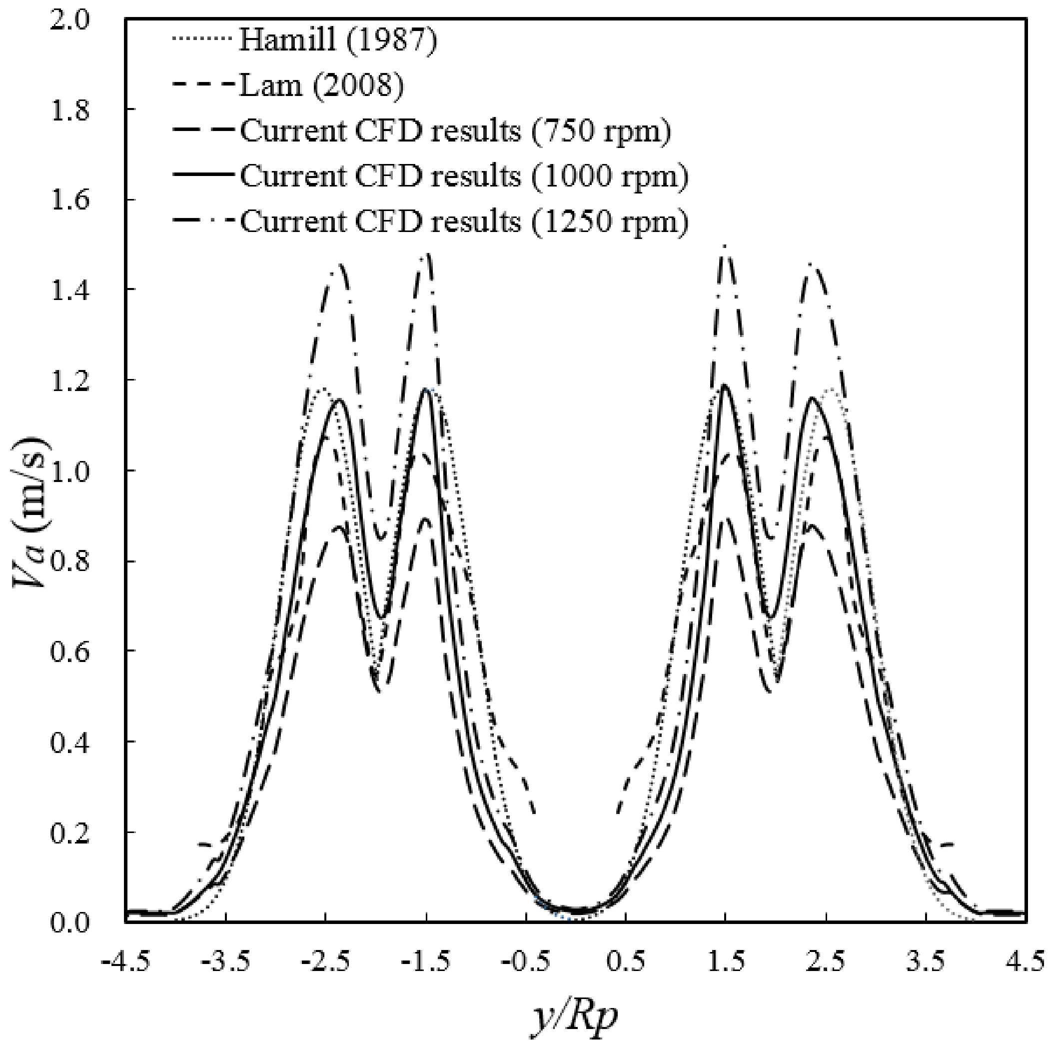

Fig. 9. Comparison of the axial velocity distribution at $1.6D_p$ within ZFE-TP-4P among the experimental result, numerical results and theoretical results.

The axial velocity distributions rotating at 750 rpm, 1000 rpm and 1250 rpm are similar at $1.6D_p$ downstream, as shown in Fig. 9. The maximum velocity values are 0.876m/s, 1.18m/s and 1.46m/s corresponding to the rotational speeds of 750 rpm, 1000 rpm and 1250 rpm respectively. It can be concluded that the maximum velocity of twin-propeller is in direct proportional to the rotational speeds within ZFE-TP-4P.

The axial velocity distribution profiles at $1.6D_p$ downstream showed similar patterns between the CFD results (1000 rpm) and the theoretical results. It can be concluded from Fig. 9 that the theoretical predicted curve at the radial distance from $\frac{y}{R_p} = -3.5$ to $\frac{y}{R_p} = -2.5$ and $\frac{y}{R_p} = 2.5$ to $\frac{y}{R_p} = 3.5$ fits the numerical curve well. The theoretical predicted curve is higher than the numerical curve within the region of $\frac{y}{R_p} = -1.5$ to $\frac{y}{R_p} = 1.5$. The experimental measurement curve is lower than the numerical curve and theoretical predicted curve. This is due to the fact that the maximum axial velocity of the experiment result is less than the numerical result, as discussed in section 4.2.

4.4.2 Two-peaked region

The axial velocity distributions within the zone of established flow of single propeller jet should also follow the general trend of the Gaussian normal probability function, Albertson *et al.* (1950). Blaauw and van de Kaa (1978) and Fuehrer and Römisch (1977) proposed Eqs. (20) and (21) based on the works of Albertson to describe the axial velocity distribution within the zone of established flow of single propeller.

$$\frac{V_{x,r}}{V_{max}} = e^{\left[-15.4\left(\frac{r}{x}\right)^2\right]} \quad \text{Eq. (20)}$$

$$\frac{V_{x,r}}{V_{max}} = e^{\left[-22.2\left(\frac{r}{x}\right)^2\right]} \quad \text{Eq. (21)}$$

Hamill (2016) agreed with Eq. (21) through the experimental validation. Fig. 10 (a)-(b) illustrate the properties of the lateral velocity distribution at $4\,D_p$ and $8\,D_p$

downstream within ZFE-TP-2P. The maximum mean velocity of the jet at each section is firstly obtained from the current CFD results (1000 rpm) and this value is used in Eqs. (20) or (21) to predict the axial velocity distribution for the twin-propeller jet.

(a)

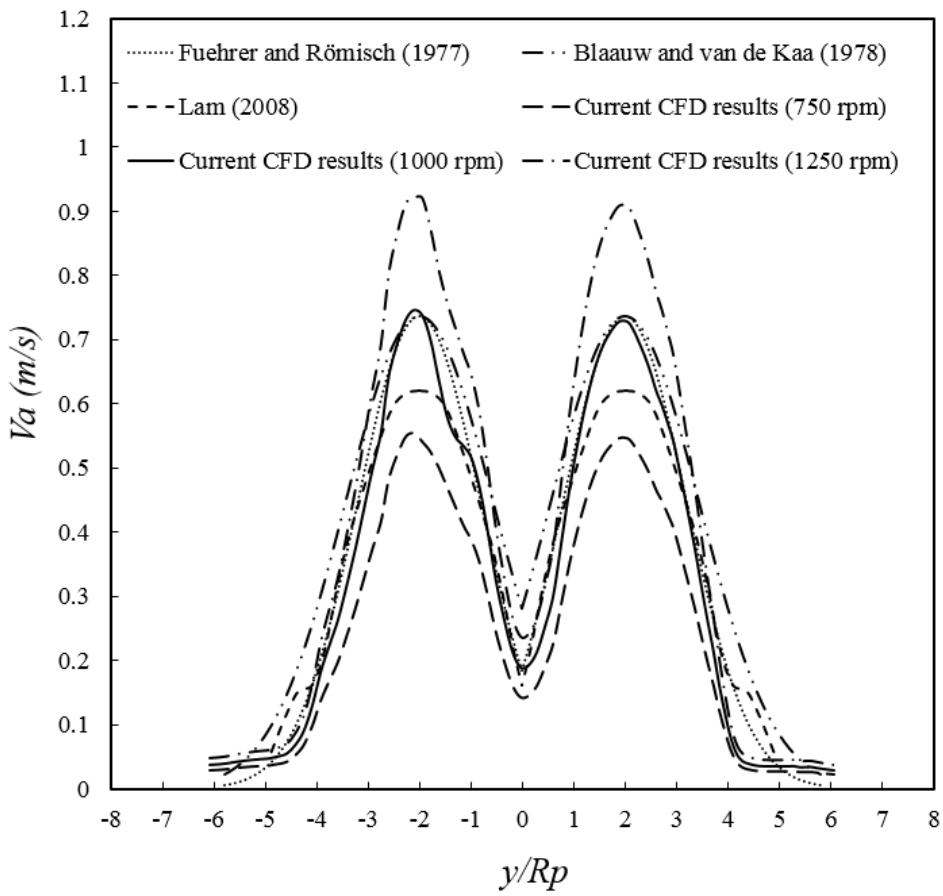

(b)

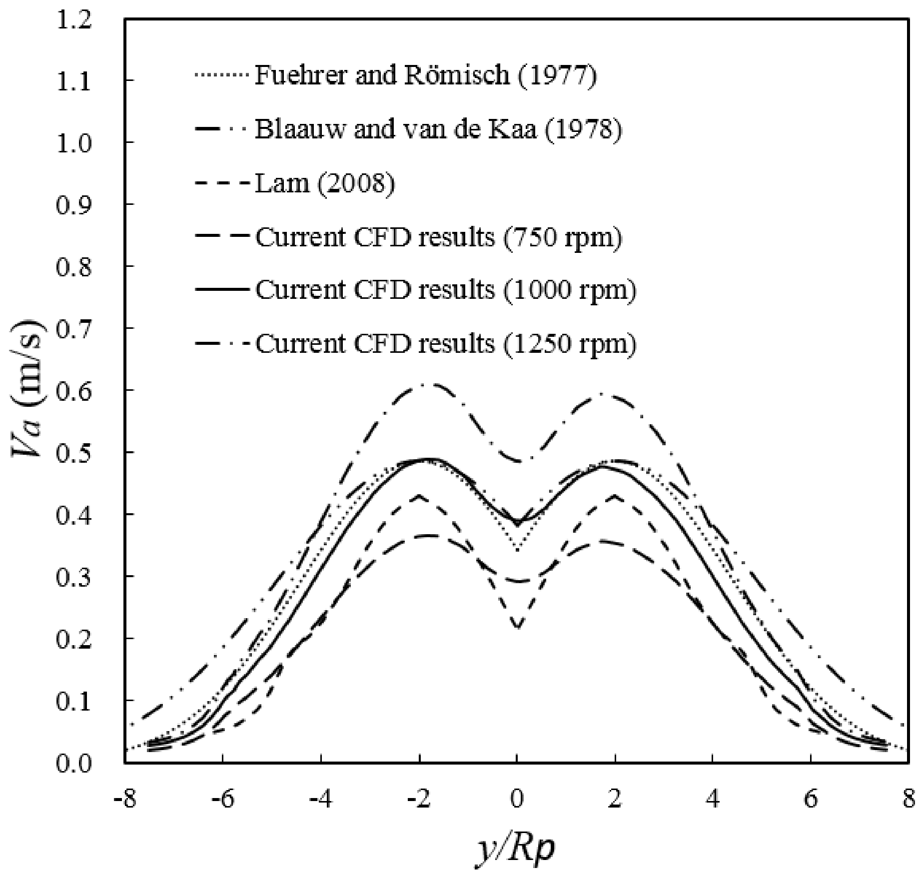

Fig. 10. Comparison of the axial velocity distribution within ZFE-TP-2P among the experimental, numerical and theoretical results. (a) $\frac{x}{D_p} = 4$; (b) $\frac{x}{D_p} = 8$

The axial velocity distributions of the three cases at 750 rpm, 1000 rpm and 1250 rpm are similar at $4D_p$ and $8D_p$ downstream, as shown in Fig. 10(a) and Fig. 10(b). The maximum velocity values are 0.55m/s, 0.75m/s and 0.92m/s corresponding to rotational speeds of 750 rpm, 1000 rpm and 1250 rpm respectively at $4D_p$ downstream. The maximum velocity values are 0.37m/s, 0.49m/s and 0.61m/s at 750 rpm, 1000 rpm and 1250 rpm at $8D_p$ downstream. It can be concluded that the maximum velocity of twin-propeller is in direct proportion to the rotational speed within ZFE-TP-2P.

Fig. 10(a) and Fig. 10(b) illustrates the properties of the axial velocity distribution at $4D_p$ and $8D_p$ downstream. Fuehrer and Römisch's (1977) equation fits better with the numerical results (1000 rpm) than Blaauw and van de Kaa's (1978). The theoretically predicted curve at the radial distance from $\frac{y}{R_p} = -6$ to $\frac{y}{R_p} = -2$ and $\frac{y}{R_p} = 2$ to $\frac{y}{R_p} = 6$ is higher than the numerical curve (1000 rpm). The numerical results (1000 rpm) suits well with the theoretically predicted curve from $\frac{y}{R_p} = -2$ to $\frac{y}{R_p} = 2$. The numerical curve (1000 rpm) is higher than the experimental curve in general. This maybe result from the interaction between two propellers.

4.5 Velocity distribution within zone of established flow

Zone of established flow of twin-propeller has only one peak value in the twin-propeller jet. Eqs. (20) and (21) are selected to compare with the numerical results at 1000 rpm. Fig. 11(a) and Fig. 11(b) illustrate the properties of the lateral velocity distribution at $14\,D_p$ and $16\,D_p$ downstream. In general, Fuehrer and Römisch's (1977) equation fits better with the numerical results than Blaauw and van de Kaa's (1978) at 1000 rpm. The jet is fully expanded and only one maximum velocity is located at the symmetrical plane. The numerical results showed the jet profile has a classical Gaussian normal distribution shape at $14\,D_p$ and $16\,D_p$ downstream.

The axial velocity distributions at 750 rpm, 1000 rpm and 1250 rpm are similar at $14D_p$ and $16D_p$ downstream, as shown in Fig. 11(a) and Fig. 11(b),. The maximum velocity values are 0.27m/s, 0.36m/s and 0.46m/s when rotating at 750 rpm, 1000 rpm and 1250 rpm at $14D_p$ downstream. The maximum velocity values are 0.26m/s, 0.35m/s and 0.43m/s when rotating at 750 rpm, 1000 rpm and 1250 rpm at $16D_p$ downstream. It can be concluded that the maximum velocity of twin-propeller is in direct proportion to the rotating speed within zone of established flow.

(a)

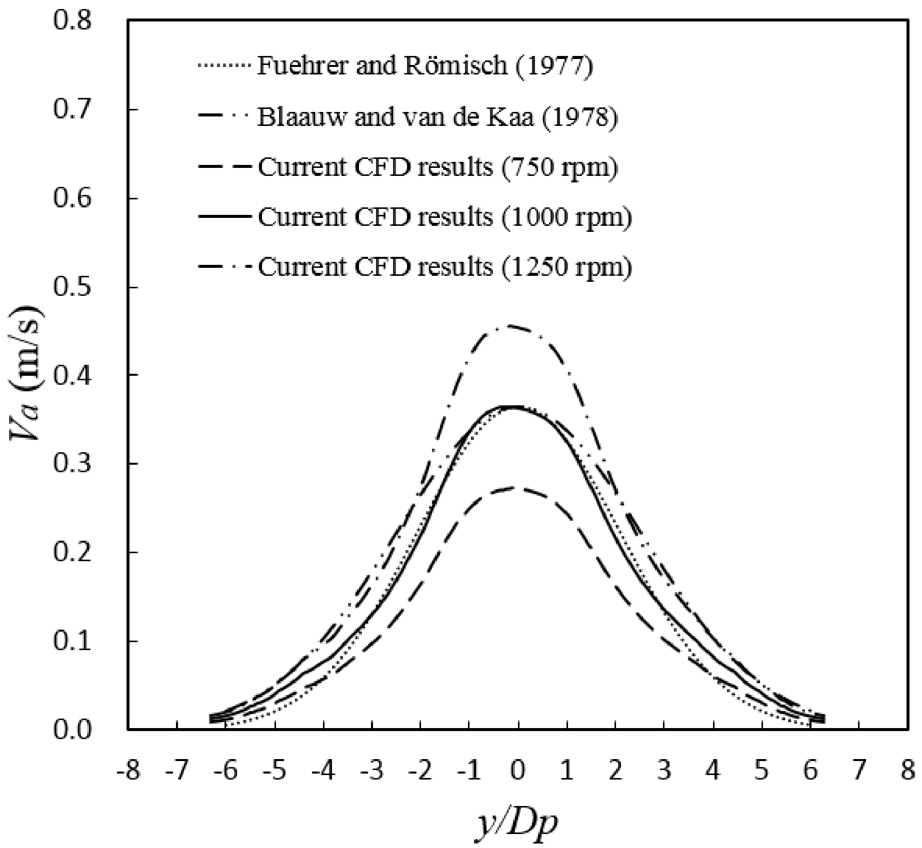

(b)

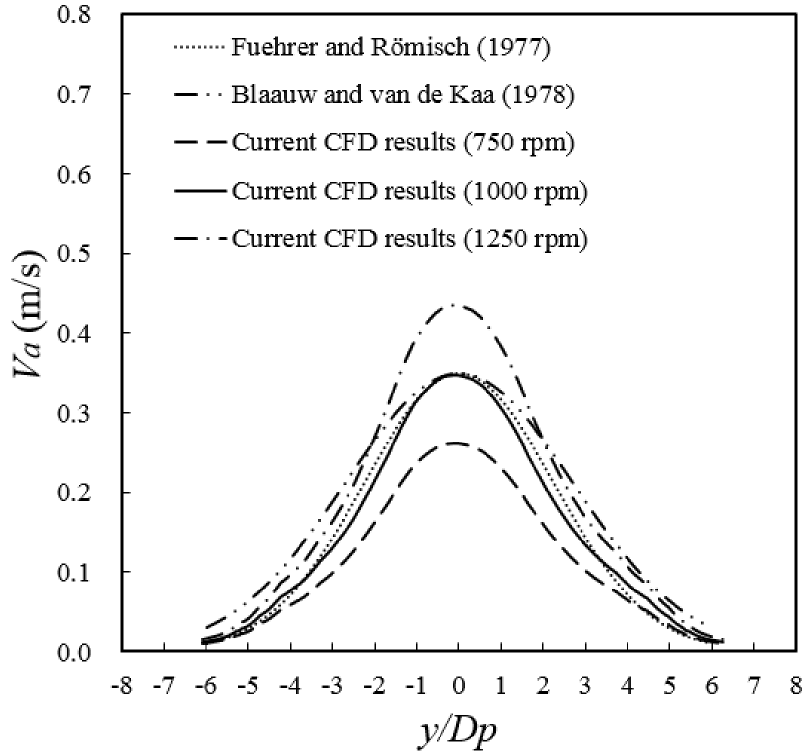

Fig. 11 Comparison of the axial velocity distribution between the numerical results and theoretical results within the zone of established flow of twin-propeller jet: (a) $\frac{x}{D_p} = 14$; (b) $\frac{x}{D_p} = 16$;

4.6 The turbulence intensities within the twin-propeller jet

Turbulence intensity is an important parameter to measure the fluctuation of time averaged velocity. Wang *et al.* (2002) indicated there is actually no distinct difference in the turbulent normal between round jets and plumes. Hamill (1987) indicated that the turbulence intensity does not increase, but decreases along the rotation axis from the propeller face. Lam (2008) measured the turbulence intensity within the zone near the efflux plane and verified Hamill's (1987) conclusion. Turbulence intensity is calculated by using Eq. (22).

$$I = \frac{\sqrt{\frac{2}{3}k}}{V_{ref}} = 0 \qquad \text{Eq. (22)}$$

where I is the turbulence intensity, k is turbulence kinetic energy which can be obtained from ANSYS Fluent™ (15.0) directly, V_{ref} is reference velocity specified by user. The local maximum velocity (V_{max}) at a particular lateral section is normally used to normalise V_{ref}.

Fig. 12(a) and Fig. 12(b) present the turbulence intensity calculated by the numerical results (1000 rpm) at x/D_p=0, 4, 8, 16 and Lam's (2008) single propeller experimental results at the efflux plane. V_{ref} is 1.5m/s, 0.81m/s, 0.52m/s and 0.36m/s when x/D_p is 0, 4, 8 and 16. It is noted that the experimental results are larger than the numerical results at the efflux plane, as shown in Fig. 12(a). This may be due to the limitations of SST k-ω turbulence to simplify the turbulent features. However, the numerical results show similar distribution as the experimental results at the efflux plane. Four peak values are found, which two peaks at the blade tips and two peaks at the hub. Rapid velocity changes at these points with high velocity gradient leading to the increase of turbulence intensity. Turbulence intensity from two propellers do not interact with each other at the efflux plane. In general, the numerical curve is lower than experimental results even having the similar distribution at the efflux plane.

The distribution of turbulence intensity changes when the jet develops downstream, as shown in Fig. 12(b),. There are 6 peak values at the efflux plane, 4 peak values at

x/D_p=4 and 8, 2 peak values at x/D_p=16. The maximum turbulence intensity decreases during the jet development downstream. It is noted that the turbulence intensity is zero at $y/R_p = 0$ at the efflux plane. Turbulence intensity is more than zero at $y/R_p = 0$ when the twin-propeller jet develops downstream. In general, the turbulence intensity has similar distribution as axial velocity within the twin-propeller jet.

(a)

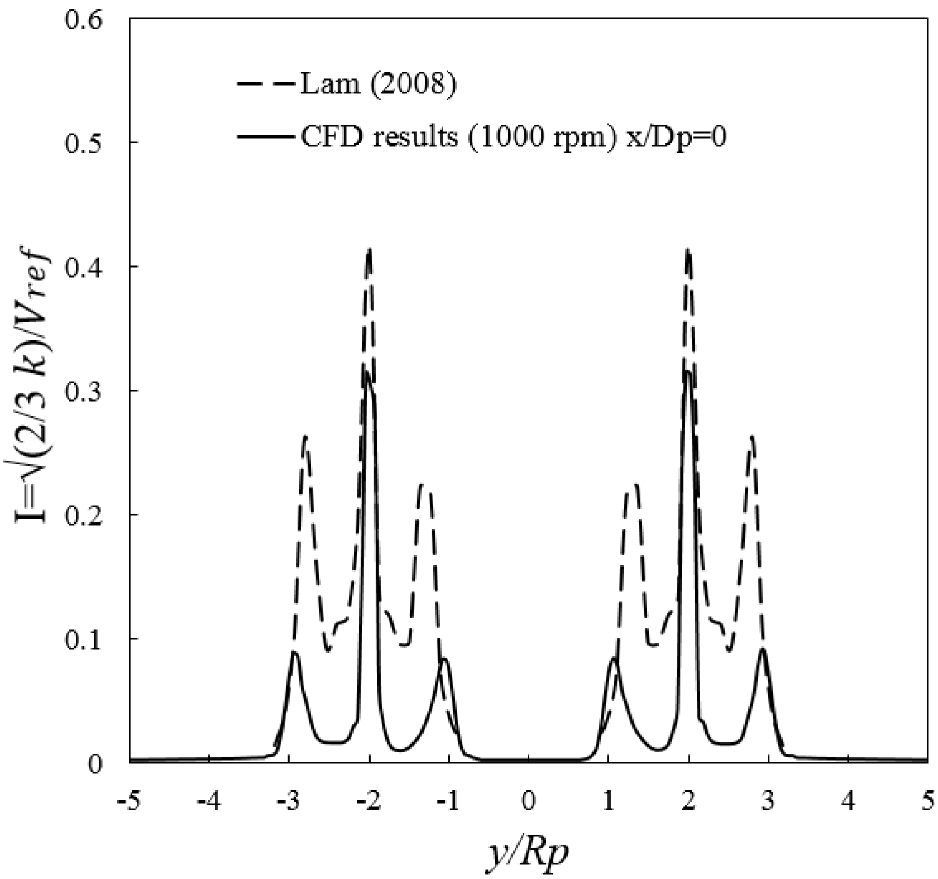

(b)

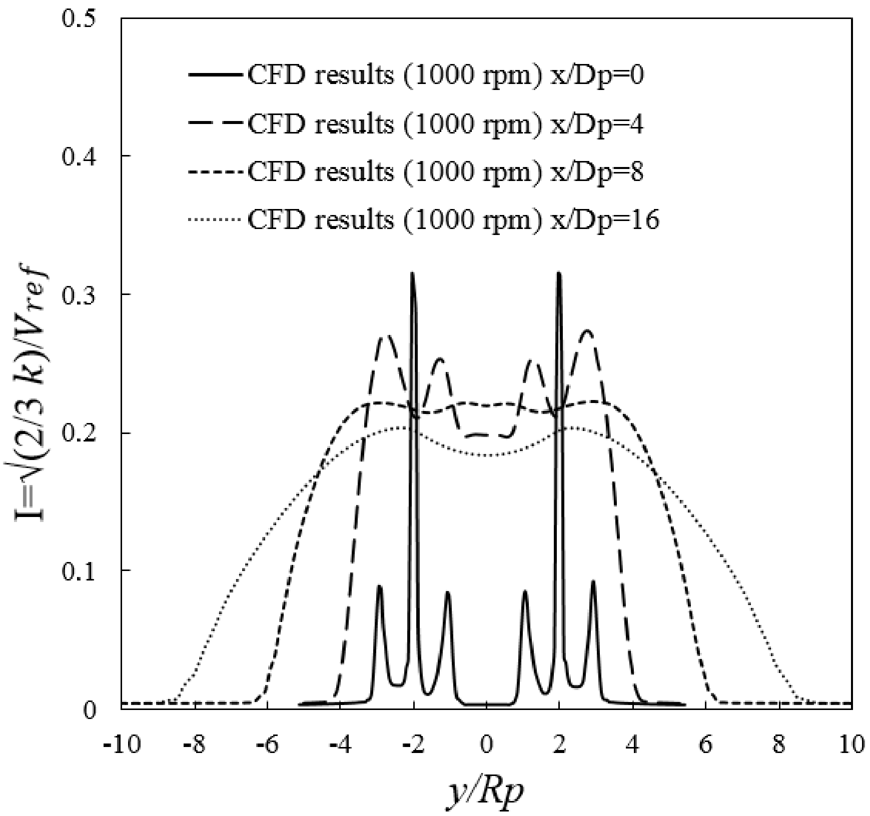

Fig. 12 The distribution of turbulence intensity within the twin-propeller jet. (a) Current CFD results (1000 rpm) and experimental results of the distribution of turbulence intensity at the efflux plane; (b) The distribution of turbulence intensity at x/D_p=0, 4, 8, 16.

4.7 Twin-propeller jet model

The flow structure of ship twin-propeller jet consists of the zone of flow establishment of twin-propeller and the zone of established flow of twin-propeller, as previously shown in Fig 6. For the time-averaged velocity, four peaks are found in the four-peak subzone (ZFE-TP-4P) and two peaks are found in the two-peak subzone (ZFE-TP-4P) within the zone of flow establishment of twin-propeller. All peak values merge into one peak within the zone of established flow of twin-propeller jet. The boundary of these two zones occurs at $x = x_{0tp}$. The numerical result shows that the zone of flow establishment ends at $x_{0tp} = 14D_p$ when the hub length (L_h) is $2D_p$.

The zone of flow establishment of twin-propeller can be further divided into two subzones according to the mixing of two propeller jets, which are the non-interference zone (ZFE-TP-NI) and interference zone (ZFE-TP-I). Two propellers do not influence each other within the non-interference zone, while two propellers jet meet at the symmetrical plane within the interference zone. The boundary of these two zones occurs at the mixing point ($x = L_{ni}$) and the length of interference zone is termed as L_i.

The zone of flow establishment of twin-propeller can also be divided into another two parts based on the peaks, which are the zone of flow establishment of twin-propeller with 4 peak values (ZFE-TP-4P) and zone of flow establishment of twin-propeller with 2 peak values (ZFE-TP-2P). ZFE-TP-4P is equivalent to the zone of flow establishment of single propeller. So the length (L_{4p}) is the same as the length of zone of flow establishment of single propeller (x_0). The numerical result shows that the length of L_{4p} is $3.5D_p$. The length of ZFE-TP-2P (L_{2p}) can be calculated by subtracting L_{4p} from x_{0tp}. Table 10 summarises the euqations used to calculate the parameters of twin-propeller jet model.

Table 10. Parameters to describe the twin-propeller jet model.

Parameter	**Equation**
Length of the zone of flow establishment of twin-propeller (x_{0tp})	$x_{0tp} = L_{ni} + L_i$
Length of ZFE-TP-NI (L_{ni})	$L_{ni} = \frac{L_t}{2*tan10^{\circ}} = 2.84L_t$
Length of ZFE-TP-I (L_i)	$L_i = x_{0tp} - L_{ni}$
Length of ZFE-TP-4P (L_{4p})	$L_{4p} = x_0$
Length of ZFE-TP-2P (L_{2p})	$L_{2p} = x_{0tp} - L_{4p}$

Previous works of single propeller are also suitable for twin-propeller jet to predict the maximum velocity and dsitrbution within the zone of flow establishment of twin-propeller through mirroring the single-propeller jet at the symtrical plane to form twin-propeller jet, as shown in Table 11.

Table 11. Proposed equations of twin-propeller jet within the zone of flow establishment of twin-propeller based on the previous single-propeller model

Type of velocity	Source	Equation
Efflux velocity (V_0)	Axial momentum theory	$V_0 = 1.59nD_p\sqrt{C_t}$
Position of maximum axial velocity at the	Berger *et al.* (1981)	$R_{mo} = 0.67(R_p - R_h)$

efflux plane (R_{mo})		
Lateral axial velocity distribution at the efflux plane	Hamill (1987)	$\frac{V_{x,r}}{V_{max}} = e^{[-(1/2)((r-R_{mo})/(R_{mo}/2))^2]}$
Axial velocity distribution within ZFE-TP-4P	Hamill (1987)	$\frac{V_{x,r}}{V_{max}} = e^{[-\frac{1}{2}\frac{(r-R_{m0})^2}{\sigma^2}]}$ $\sigma = \frac{1}{2}R_{m0}$, for $x/D_p < 0.5$ $\sigma = \frac{1}{2}R_{m0} + 0.075\left(x - \frac{D_p}{2}\right)$, for $x/D_p > 0.5$
Axial velocity distribution within ZFE-TP-2P	Fuehrer and Römisch (1977)	$\frac{V_{x,r}}{V_{max}} = e^{[-22.2\left(\frac{r}{x}\right)^2]}$
Magnitude of the maximum axial velocity decay within ZFE-TP-4P	Hamill (2016)	$0 \leq x/D_p < 0.35$ $\frac{V_{max}}{V_0} = 1$ $0.35 \leq x/D_p < 3.25$ $\frac{V_{max}}{V_0} = 1.51 - 0.175\left(\frac{x}{D_p}\right) - 0.46P'$
Magnitude of the Magnitude of the maximum axial velocity decay within ZFE-TP-2P	Verhey (1983)	$1.5 \leq x/D_p$ $\frac{V_{max}}{V_0} = 1.275(x/D_p)^{-0.7}$

All the peak values merge into one at the symmetrical plane within the zone of established flow of twin-propeller. The magnitude of the maximum axial velocity decay within the zone of established flow of twin-propeller can be calcualted by using the Jiang and Lam equation proposed in this paper. Fuehrer and Römisch (1977)'s equation (Eq. 21) from single-propeller model is suitable to predict the axial velocity distribution within the zone of established flow of twin-propeller with the summary in Table 12 to predict the twin-propeller jet model within the zone of established flow of twin-propeller.

Table 12. Equations to predict the twin-propeller jet model within the zone of established flow of twin-propeller.

Type of velocity	**Source**	**Equation**
Maximum axial velocity decay within the zone of established flow of twin-propeller	Jiang and Lam (2018)	$\frac{V_{max}}{V_0} = 1.8(\frac{x}{D_p})^{-0.7}$
Axial velocity distribution within the zone of established flow of twin-propeller	Fuehrer and Römisch (1977)	$\frac{V_{x,r}}{V_{max}} = e^{[-22.2(\frac{r}{x})^2]}$

5. Conclusions

The research works demonstrated the investigation the flow characteristics of the ship twin-propeller jet based on the understanding of the single propeller jet. Computational Fluid Dynamics (CFD) is successfully implemented to further understand the velocity distribution within the jet. Twin-propeller jet model is proposed to enable the prediction of the velocity field within the zone of flow establishment and the zone of established flow from the ship with twin propellers. The proposed findings are:

1. Twin-propeller jet has been divided to be zone of flow establishment and zone of established flow as two zones in single-propeller jet. Zone of the flow establishment is the initial zone close to the propeller and followed by the zone of established flow.
2. Efflux velocity of twin-propeller, which is the maximum velocity at the efflux plane, is the same as two non-interfering single propellers. Equation to predict the efflux velocity of single propeller can be used to predict the efflux velocity in twin-propeller jet as $V_0 = 1.59nD_p\sqrt{C_t}$.
3. Velocity distribution of the efflux velocity plane can be predicted using the equation proposed by Hamill (1987) $\frac{V_{x,r}}{V_{max}} = e^{[-(1/2)((r-R_{mo})/(R_{mo}/2))^2]}$ and the position of the efflux velocity can be predicted using the equation proposed by Berger *et al*. (1981) $R_{mo} = 0.67(R - R_h)$.
4. Twin-propeller jet is symmetrical about the central plane ($D_{tp}/2$) in the zone of flow establishment and the zone of established flow.

5. Zone of flow establishment can be divided to be non-interfering region and interfering region. Twin-propeller jet can be treated as two single-propeller jets in non-interfering region within the zone of flow establishment. Four peaks are shown in non-interfering zone without interference.
6. In interfering region of zone of flow establishment, two propeller jets interfered each other producing a four-peaked ridge. This four-peaked ridge merged to be two-peaked ridge in the interfering region at $x = 3.5D_p$.
7. Length of the zone of flow establishment is the distance between the starting point at efflux plane and the end of this zone. Starting point is counted from the efflux plane and the end of the zone of flow establishment of twin-propeller jet occurs at $14D_p$ when the value of L_h is $2D_p$, at which position all of the four peak values merge into one peak.
8. Selected single-propeller jet equations are suggested to predict the velocity field of twin-propeller jet within the zone of flow establishment including,
   a) Decay of velocity by Hamill (2016)

$$\frac{V_{max}}{V_0} = 0.964 - 0.039\left(\frac{x}{D_p}\right) - 0.344P'$$

   b) Decay of velocity by Verhey (1983)

$$\frac{V_{max}}{V_0} = 1.275(x/D_p)^{-0.7}$$

   c) Velocity distribution by Hamill (1987)

$\frac{V_{x,r}}{V_{max}} = e^{[-\frac{1}{2}\frac{(r-R_{m0})^2}{\sigma^2}]}$, when $\frac{x}{D_{sp}} < 0.5$, $\sigma = \frac{1}{2}R_{m0}$ and when $\frac{x}{D_p} > 0.5$, $\sigma = \frac{1}{2}R_{m0} + 0.075\left(x - \frac{D_p}{2}\right)$

   d) Velocity distribution by Fuehrer and Römisch (1977)

$$\frac{V_{x,r}}{V_{max}} = e^{[-22.2\left(\frac{r}{x}\right)^2]}$$

9. Zone of established flow shows one peaked ridge after the end of the zone of flow establishment.
10. The maximum of velocity of twin-propeller jet is located at the central plane in the zone of established flow compared to the rotational axis for single-propeller jet. An equation for velocity decay is proposed associated with the use of velocity distribution equation from the previous research. Two equations are suggested to predict the decay and axial velocity distribution of the twin-propeller jet.
    a) Decay of velocity at central plane by current study as Jiang and Lam equation,

    $$\frac{V_{max}}{V_0} = 1.8\left(\frac{x}{D_p}\right)^{-0.7}$$

    b) Velocity distribution by Fuehrer and Römisch (1977),

    $$\frac{V_{x,r}}{V_{max}} = e^{[-22.2\left(\frac{r}{x}\right)^2]}$$

11. The efflux velocity and maximum velocity of twin-propeller at each cross section are in direct proportion to the rotating speed of the propeller as single propeller. The maximum velocity decay and the axial velocity distribution of twin-propeller jet is independent of the speed of rotation within the twin-propeller jet. The length of each zones are not influenced by the rotating speed.
12. The maximum turbulence intensity at each cross section decreases while the range of maximum turbulence intensity increases as the twin-propeller jet develop downstream.

Acknowledgements

The current research was supported by the fund of Tianjin Natural Science Foundation (18JCYBJC21900), Beiyang Scholar Foundation and State Key Laboratory of Hydraulic Engineering Simulation and Safety from Tianjin University, People's Republic of China. The authors wish to extend their gratitude to Queen's University Belfast, University of Plymouth, University of Oxford, Dalian University of Technology, University of Malaya, University Technology Malaysia and Southern University College for the previous financial supports. Heartiest appreciation to those scientists and engineers from Energy Institute, Engineers Ireland, British Computer Society, The Institution of Engineering and Technology, The Institute of Engineers Malaysia and Malaysian Invention & Design Society for direct and indirect inputs to our long-term research works. Thank you for Marine Renewable Energy (MREL) at Tianjin University for facilities.

Nomenclature

D_p	Propeller diameter
D_h	Hub diameter
N	Blade number
θ	Rake angle
P'	Pitch ratio
β	Blade area ratio
C_t	Thrust coefficient
L_h	Distance from hub to hub
D_{tp}	Width of twin-propeller
R_p	Propeller radius
R_h	Propeller hub radius
r	Radial distance from the axis
V_0	Efflux velocity
n	The rotate speed of propeller in rev/s
$V_{x,r}$	The mean velocity at any position in the jet
V_{max}	The maximum velocity of the cross section
R_{mo}	The radius distance from the rotating axis to the point of maximum axial velocity at the efflux plane
x_0	The length of the zone of flow establishment of single propeller
x_{0tp}	The length of the zone of flow establishment of twin-propeller

L_{ni}	The length of none interference zone
L_i	The length of interference zone
σ	Standard deviation
y	Distance from the symmetrical plane
L_{4p}	The length of ZFE-TP-4P
L_{2p}	The length of ZFE-TP-2P
I	Turbulence intensity
k	Turbulence kinetic energy
V_{ref}	Reference velocity
ρ	The density of fluid

References

Albertson, M. L., Dai, Y. B., Jensen, R. A., Rouse, H. (1950). "Diffusion of submerged jets." American Society of Civil Engineers, Vol. 115, No. 11, pp. 639-664.

ANSYS ICEM (2013). "ANSYS ICEM CFD user's manual 15.0." ANSYS Inc., Canonsburg, Pennsylvania.

ANSYS Fluent (2013). "ANSYS Fluent user's guide 15.0." ANSYS Inc., Canonsburg, Pennsylvania.

Berger, W., Felkel, K., Hager, M., Oebius, H., Schale, E. (1981). "Courant provoque parles bateaux protection des berges et solution pour eviter l'erosion du lit duhaut rhin." Proceedings of 25th Congress P.I.A.N.C., Section 1-1. Edinburgh.

Blaauw, H. G., van de Kaa, E. J. (1978). "Erosion of bottom and sloping banks caused by the screw race of manoeuvring ships." Delft Hydraulics Laboratory, Delft, Netherlands, Publication No. 202, pp. 1–12.

Fuehrer, M., Romisch, K. (1977). "Effects of modern ship traffic on islands and ocean waterways and their structures." Proceedings of 24th Congress P.I.A.N.C., Sections 1–3, Leningrad.

Hamill, G. A. (1987). "Characteristics of the screw wash of a manoeuvring ship and the resultant bed scour." Thesis submitted to the Queen's University of Belfast for the degree of Doctor of Philosophy.

Hamill, G. A., Kee, C., Ryan, D. (2015). "3D efflux velocity characteristics of marine propeller jets." Proceedings of the ICE - Maritime Engineering, Vol. 168, No. 2, pp. 62-75, DOI: 10.1680/maen.14.00019.

Hamill, G. A., Kee, C. (2016). “Predicting axial velocity profiles within a diffusing marine propeller jet.” Ocean Engineering, Vol. 124, pp. 104-112, DOI: 10.1016/j.oceaneng.2016.07.061.

Johnston, H. T., Hamill, G. A., Wilson, P. R., Ryan, D. (2013). “Influence of a boundary on the development of a propeller wash.” Ocean Engineering, Vol. 61, pp. 50-55, DOI: 10.1016/j.oceaneng.2012.12.033.

Lam, W. (2008). “Simulations of a ship's propeller jet.” Thesis submitted to the Queen’s University of Belfast for the degree of Doctor of Philosophy.

Lam, W., Hamill, G. A., Song, Y. C., Robinson, D. J., Raghunathan, S. (2011). “Experimental investigation of the decay from a ship's propeller.” China Ocean Engineering, Vol. 25, No. 2, pp. 265-284, DOI: 10.1007/s13344-011-0050-5.

Lam, W., Hamill, G. A., Robinson, D., Raghunathan, S., Song, Y. (2012). “Analysis of the 3D zone of flow establishment from a ship propeller.” KSCE Journal of Civil Engineering, KSCE, Vol. 16, No. 4, pp. 465-477, DOI: 10.1007/s12205-012-1256-7.

Lam, W., Hamill, G. A., Robinson, D.J. (2013). “Initial wash profiles from a ship propeller using CFD method.” Ocean Engineering, Vol. 72, pp. 257-266, DOI: 10.1016/j.oceaneng.2013.07.010.

Lee, J. H. W., Chu, V. H. (2003). “Turbulent jets and plumes: a Lagrangian approach.” Kluwer Academic, Netherlands, DOI: 10.1007/978-1-4615-0407-8.

Mujal-Colilles, A., Gironella, X., Crespo, A. J. C., Sanchez-Arcilla, A. (2017). “Study of the bed velocity induced by twin propellers.” Journal of Waterway Port Coastal and Ocean Engineering, Vol. 143, No. 5, 04017013-8. DOI:

10.1061/(ASCE)WW.1943-5460.0000382.

Prosser, M. (1986). “Propeller induced scour.” Tech. rep., BHRA Project RP A01415, The Fluid Engineering Centre, Cranfield.

Solidworks (2016). “Solidworks tutorials 2016.” Dassault Systèmes Solidworks Corporation, Concord, Massachusettss.

Stewart, D. P. J. (1992). “Characteristics of a ship's screw wash and the influence of quay wall proximity.” Thesis submitted to the Queen’s University of Belfast for the degree of Doctor of Philosophy.

Verhey, H. J. (1983). “The stability of bottom and banks subjected to velocities in the propeller jet behind ships.” Delft Hydraulics Laboratory, Netherlands, Delft Publication No. 303, pp.1–11.

Versteegs, H. K., Malalasekera, W. (2007). “An introduction to computational fluid dynamics the finite volume method.” Second Edition, Prentice Hall, Essex, England.

Wang, H., Law, A. W. K. (2002). “Second-order integral model for a round turbulent buoyant jet.” Journal of Fluid Mechanics, Vol. 459, pp. 397-428, DOI: 10.1017/S0022112002008157.